Adsorption (2011) 17: 385–394
DOI 10.1007/s10450-011-9335-5

Evaluation of the interaction potentials for methane adsorption on graphite and in graphitic slit pores

Mus'ab Abdul Razak · D.D. Do · G.R. Birkett

Received: 5 May 2010 / Accepted: 7 February 2011 / Published online: 23 February 2011

Abstract This paper compares the performance of the Buckingham Exponential-6 and Lennard-Jones potential models in the description of bulk phase and adsorption properties of methane on graphitic surfaces and pores. The solid-fluid potential used in the choice of the LJ model is Steele 10-4-3 equation and for the Exp-6 model, the Crowell and Chang equation which has been rarely used in the literature. From an extensive computer study using Grand Canonical Monte Carlo simulation, the two potential models perform almost equally well in the bulk fluid behavior except at extremely high density, where the LJ model is better. For adsorption on surface, the Exp-6 performs better in the correct description of the experimental Henry constant. However, both potential models describe well the isotherm outside the Henry law region. Under supercritical conditions, the same behavior is seen in the Henry law region, but the opposite is observed at extremely high pressures. For adsorption in slit pores, significant difference is seen at low pressure region for all pore sizes examined. In this region, the Exp-6 always predicts a higher capacity than the LJ model. In the smallest pore size examined (0.65 nm), the LJ model predicts a higher capacity than the Exp-6 with approximately 4% difference at higher pressures. However, this behavior is not seen in the other pore sizes. The comparison shows that the Exp-6 can describe experimental adsorption data, albeit only, better than the LJ.

Keywords Lennard-Jones · Buckingham Exp-6 · Gas phase adsorption · Graphite · Methane

M. Abdul Razak · D.D. Do (✉) · G.R. Birkett
School of Chemical Engineering, University of Queensland, St. Lucia, Qld 4072 Australia
e-mail: d.d.do@uq.edu.au

1 Introduction

Adsorption of gases and liquids on solid surfaces and porous materials, such as activated carbon, has been extensively studied in the literature. Its understanding has increased due to the development of molecular simulation methods such as Monte Carlo (MC), molecular dynamics (MD) (Allen and Tildesley 1989; Frenkel and Smit 1996) and density functional theory (DFT). Grand Canonical Monte Carlo simulation (GCMC) is the most widely used method because it mimics the same conditions that are generally used in an adsorption experiment where the temperature, volume, and chemical potential, via pressure in the bulk phase, are specified (Nicholson and Parsonage 1982). Whilst the choice between different Monte Carlo ensembles is generally one of convenience, the choice of the molecular potential used is critically important.

Most of the studies on adsorption in the literature are limited to the use of the Lennard-Jones model (LJ) to describe the dispersive interaction between fluids. There are many other models that are available but the LJ model is preferred for adsorption on a carbon surface because it is consistent with the usage of the well-known Steele model for fluid-solid interaction (Steele 1973) and its molecular parameters are more readily available in the literature. The LJ model has inverse 12-power dependence for the repulsive interaction on intermolecular separation, which is chosen for mathematical convenience and has no physical basis (Kaplan and Piela 2007; Wu and Sadus 2000; Galliero and Boned 2008). Such weakness may be of importance because the structural properties of a simple fluid are partly determined by the intermolecular short range repulsion interactions. Although it is convenient, the LJ model is found to be inadequate in some conditions (Wu and Sadus 2000).

Some researchers have utilized the Buckingham Exp-6 model (Exp-6) (Buckingham 1938), which describes the repulsion interaction through an exponential form, in place of the LJ model. This description of repulsion is more consistent with both quantum mechanical *ab initio* calculations and analysis of experimental data on simple molecular systems than the inverse-power form (Ree 1983). Furthermore, the advantage of the Exp-6 model over the LJ counterpart model is the additional parameter, α. This parameter describes the stiffness of the repulsion for which the LJ clearly lacks, and it is because of this parameter the Exp-6 model is shown to describe more accurately than LJ model the coexistence data of methane (Errington and Panagiotopoulos 1998). Since the repulsion plays a significant role under extremely high pressures, it is generally expected that this is where the two potential models would differ. It will be shown in this paper that the difference can occur at conditions other than the extremely high pressure conditions. Recent studies have shown increased attention on the model, for example high pressure behavior by Vortler (1997), mixtures by Wu and Sadus (2000), phase behavior of pure fluids by Tavares and Sandler (1996) and Errington and Panagiotopoulos (1998), and gas-gas equilibria by Zarragoicoechea and Scalise (1997). Furthermore, Paricaud et al. (2005) have reported that the Exp-6 model works better than the LJ model in matching the microstructure of water with high accuracy. These researches have provided evidence that the Exp-6 model has some significant advantages for molecular simulation.

This work will focus on the comparison between Exp-6 and LJ models with their corresponding fluid-solid interaction potential model, which are Crowell-Chang model (1963) and Steele model, respectively. The main difference between these two models is the short range repulsion interaction, which plays a significant role on the structural properties of simple gases. Methane will be used in this work because of the interest in natural gas storage and transportation and because it can be modeled as single site sphere in simulation. In this paper, the performance of these two potential models, LJ and Exp-6, are studied in description of bulk fluid behavior and in description of adsorption behavior of methane on the graphitic surfaces and pores. The details of the GCMC simulation for methane will be described in the next section.

2 Theory

2.1 GCMC simulation

In this work, the bulk phase analysis results were obtained using the NVT ensemble, while the adsorption isotherm and isosteric heat of methane on graphitized carbon black were obtained by GCMC simulation. In NVT-ensemble, the density and the temperature are specified to obtain the bulk pressure of the system. In the GCMC-ensemble, the temperature, volume and chemical potential are specified. The conversion of the chemical potential to pressure is obtained by using the Wagner Equation of State (Setzmann and Wagner 1991).

In the Monte Carlo simulation, 30,000 cycles are used for the equilibrium step and another 30,000 cycles are used for the collection of statistics. Each cycle consists of one thousand attempted displacements, insertions or deletions with equal probability. The box lengths were chosen depending on the condition used, and the periodic boundary conditions are applied except at the surface or at the pore walls. The cutoff radius is taken to be either 5 times the collision diameter or half of the box length, whichever is smaller. The displacement step is always set initially as half of the box length and is adjusted to achieve an acceptance ratio of 50%.

2.2 Fluid-fluid interaction potential

In adsorption, there are two components contributing to the interaction potential; the fluid-fluid interaction and the fluid-solid interaction. The most commonly used fluid-fluid interaction potential model is the Lennard-Jones model (Do and Do 2005) because it is relatively simple and its parameters are readily available for a wide range of fluids. However, it is important to note that the LJ model is an empirical equation that approximately reproduces the dispersion interaction between atoms. The model is described as:

$$\varphi_{ff}(r) = 4\varepsilon_{ff}\left[\left(\frac{\sigma_{ff}}{r}\right)^{12} - \left(\frac{\sigma_{ff}}{r}\right)^{6}\right] \tag{1}$$

where ε_{ff} is the well depth of the interaction potential and σ_{ff} is the collision diameter. In this model, the repulsion term is significant when the r is smaller than σ_{ff}.

The Buckingham Exp-6 model is defined by:

$$\begin{cases} \varphi_{ff}(r) = \dfrac{\varepsilon_{ff}}{(1-\frac{6}{\alpha})}\left[\dfrac{6}{\alpha}\exp\left(\alpha\left(1-\dfrac{r}{r_m}\right)\right) - \left(\dfrac{r_m}{r}\right)^6\right], \\ \quad r \geq r_{\min} \\ \varphi_{ff}(r) = \infty, \quad r < r_{\min} \end{cases} \tag{2}$$

where ε_{ff}, r_m, and α are model parameters. ε_{ff} is the well depth, r_m is the radial distance at which the potential is minimum and α represents the stiffness of the repulsion component of the potential. $r_{\min}$ is the smallest positive value for which $d\varphi_{ff}(r)/dr = 0$. The second condition is necessary because the potential will decrease when $r < r_{\min}$ and become negative as the distance approaches zero (Errington and Panagiotopoulos 1998). The clear distinction between this model and the LJ model is the repulsion part, which could cause significant difference in the calculation of the

Table 1 Molecular interaction parameters

		E (K)	σ (nm)	r_m (nm)	r_{max} (nm)	α	A (K nm^6)	B (K)	α' (nm^{-1})
LJ	Methane	148.0	0.373						
	Graphite	28.0	0.340						
Exp-6	Methane	160.3	0.374	0.4188	0.07108	15.0	1.442	3.493×10^8	35.8
	Graphite	30.98		0.3827		13.7	0.173	2.152×10^7	35.8

total energy of interaction and thus, the adsorption isotherm and the isosteric heat.

Since the LJ model is popular and simple, there are many different sets of parameters that are reported in the literature for methane (Martin and Siepmann 1998; Duan et al. 2000). Do and Do (2005) have studied different sets of parameters for simple gases in describing adsorption on carbon black. They have found the best parameters for methane which are summarized in Table 1. The Exp-6 potential model, however, has received less attention. The molecular parameters for this potential can be found from Sherwood (1964), and Ross and Ree (1980) for several gases. Recently, Errington and Panagiotopoulos have optimized the Exp-6 parameters for methane by fitting the simulation results against the vapor-liquid coexistence data (Errington and Panagiotopoulos 1998). These parameters will be used in this work and are listed in Table 1.

2.3 Fluid-solid interaction potential

The graphite surface is modeled as a homogeneous semi-infinite plane. While the intermolecular interaction between two methane molecules is described by the LJ model, the corresponding fluid-solid interaction is described by the Steele model (1973):

$$\varphi_{sf}(z) = 4\pi\varepsilon_{sf}\rho_s\sigma_{sf}^2\left[\frac{1}{5}\left(\frac{\sigma_{sf}}{z}\right)^{10} - \frac{1}{2}\left(\frac{\sigma_{sf}}{z}\right)^{4} - \frac{\sigma_{sf}^4}{6\Delta(z+0.61\Delta)^3}\right] \tag{3}$$

where ρ_s is the density of solid. The value of ρ_s and Δ for graphite are 38.2 nm^{-2} and 0.3354 nm, respectively. σ_{sf} and ε_{sf} are the fluid-solid LJ molecular parameters and, z is the shortest distance between the fluid particle and the solid surface. Although the model neglects the lateral variation along the graphite plane, it gives reasonable approximation of the interaction with the solid (Kowalczyk et al. 2005).

The Crowell-Chang model is used to describe the fluid-solid interaction for Exp-6 fluids. The interaction is given by (4) at a distance z from the outer basal plane of a semi-infinite lattice.

$$\varphi_{sf}(z) = -\left(\frac{A_{sf}\pi\eta}{12\Delta^4}\right)\psi^{(3)}(x) + B_{sf}\left[\frac{2\pi\eta}{\alpha_{sf}'^2}\right](\alpha_{sf}'z+1)e^{-\alpha_{sf}'z} \tag{4}$$

In this model, A_{sf}, B_{sf}, and α_{sf}' are the molecular parameters. The parameters were derived from the original Exp-6 model as shown in Appendix A.1. Δ is the interlayer spacing in graphite, η is the number of carbon atoms per unit area in the basal plane, $x = z/\Delta$ and $\psi^{(3)}(x)$ is the pentagamma function tabulated by Davis (1963). Equation (5) defines the pentagamma function in a power series form.

$$\psi^{(3)}(x) = 3!\sum_{k=0}^{\infty}\frac{1}{(x+k)^4} \tag{5}$$

To reduce the computation time in the GCMC simulation this pentagamma function is approximated by:

$$\psi^{(3)}(x) \cong 3!\left[\frac{1}{x^4} + \frac{1}{3(x+0.6)^3}\right] \tag{6}$$

The accuracy of this approximation is given in Appendix A.2. Fluid-solid interaction parameters for both models were calculated by applying the Lorentz-Berthelot (LB) mixing rules on the molecular parameters listed in Table 1.

2.4 Accessible pore volume and width

The accessible pore volume is defined as the volume in which methane particles can access. The fluid-solid potential between a methane molecule on the boundary of this accessible volume and the pore wall is zero (Birkett and Do 2006). The accessible volume can be calculated using (7).

$$V_{acc} = A(H - 2z_0) \tag{7}$$

where z_0 is the shortest distance from the pore wall, at which the solid-fluid potential energy is zero, H is the physical width of the pore, and A is the area of one wall of the pore.

2.5 Isosteric heat

One of the thermodynamic quantities of interest that can be readily obtained from GCMC simulation is the isosteric heat. It can be calculated (Nicholson and Parsonage 1982),

$$q_{st} = kT + \left[\frac{\langle U_{ff}\rangle\langle N\rangle - \langle U_{ff}N\rangle}{\langle N^2\rangle - \langle N\rangle\langle N\rangle}\right] + \frac{\langle U_{sf}\rangle\langle N\rangle - \langle U_{sf}N\rangle}{\langle N^2\rangle - \langle N\rangle\langle N\rangle} \quad (8)$$

where $\langle\,\rangle$ is the ensemble average, N is the number of particles, and U_{ff} and U_{sf} are the interaction potentials from the fluid-fluid and the fluid-solid contributions.

2.6 Local density distribution

The local density distribution show, in a 2D-plot, the distribution of fluids from the graphite surface or pore wall, which helps to understand how particles are structured in the adsorbed layers. It is defined as:

$$\rho(z) = \frac{\langle \Delta N(z)\rangle}{L_x L_y \Delta z} \quad (9)$$

where $\Delta N(z)$ is the number of fluids whose centers of mass are located in the segment having boundaries at $z - 0.5\Delta z$ and $z + 0.5\Delta z$ and L_x and L_y and are the box lengths in the x- and y-directions, respectively.

3 Results and discussion

3.1 Lennard-Jones model and Exponential-6 model

Methane pair interaction for both models was first analyzed to give an idea of the difference between the two models. Figure 1 shows methane pair-wise fluid-fluid interactions for both models with respect to distance. It shows that there is a difference in the fluid-fluid interaction between two models. The Exp-6 model has a steeper repulsion than the LJ model. It also has a greater well depth (see the inset of Fig. 1). It is important to point out that in the literature Exp-6 model has been reported to be less steep than the LJ model (Vortler et al. 1997; Ross and Ree 1980). The dissimilarity is due to the repulsive stiffness α, which can vary depending on the optimization of the molecular parameters.

To further illustrate the difference, the bulk isotherms of methane under supercritical conditions were generated and analyzed. In Fig. 2 the isotherms of both models agree with the experimental data (Linstrom and Mallard 2001) except at high densities, where the Exp-6 model deviates from the experimental data. At density of 35.5 kmol/m^3, the percentage error in the pressure of the Exp-6 model data goes up to

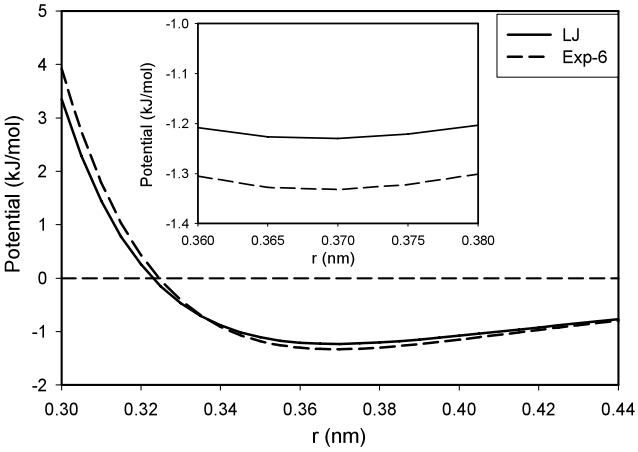

Fig. 1 Potential model of interaction between two methane particles. The *inset* shows the minimum of the potential energy of both models

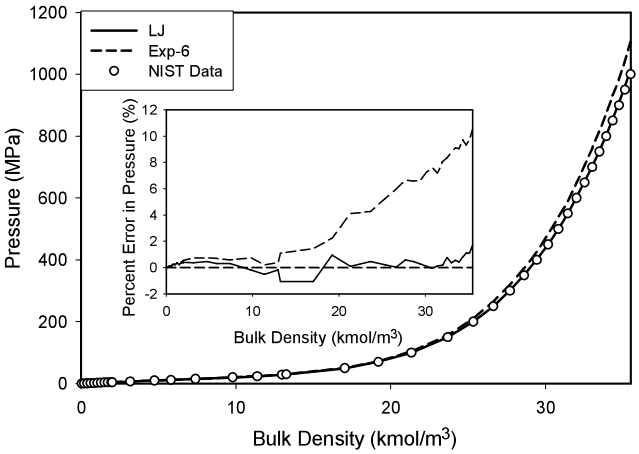

Fig. 2 The bulk pressure of methane at 298.15 K. The *inset* shows the percentage error between both models and the NIST data

10.5%, as seen in the inset of Fig. 2. This difference shows the effect of the repulsion stiffness of the two models. From the results, it can be concluded that both models are able to describe the experimental data well; however, LJ model can describe the experimental data better at higher densities.

3.2 Steele model and, Crowell-Chang model

In fluid-solid interaction, the difference between the well depths of the two models is about 2.5%. Figure 3 shows that the Crowell-Chang model has a softer repulsion than the Steele potential. To see the effects of this softer repulsion, two cases were considered; first is the adsorption in ultra fine pores, where only one molecular layer is possible, whereas, the second is the adsorption under extremely high pressure. The first case is to study the effects of the solid-fluid interaction directly so that the repulsive contribution of this interaction can be evaluated. In the second case both

the fluid-fluid and fluid-solid interaction will be analyzed simultaneously to investigate the interplay between the two interactions.

Before analyzing the isotherms and the isosteric heat, the accessible pore width were checked to see how the two models affect the accessibility of methane particles in pores. The results of this analysis for different pore sizes are shown in Table 2. It can be seen that, as the pore size increases, the difference of the accessible pore width between the two models decreases.

Figure 4 illustrates the adsorption isotherms of methane on a graphitized carbon black surface at 113, 123, 133, and 143 K. The inset shows the percentage error between the two models and the experimental data (Bezus et al. 1967; Avgul and Kiselev 1970). It is observed that the Exp-6 model predicts a higher Henry constant and this is simply due to the greater well depth of the fluid-solid contribution of this model (see inset in Fig. 3). Although the difference in the well depth of the two models is 2.5%, the adsorption capacity predicted by the Exp-6 model adsorption can be up to 55% higher than the LJ model at 113 K. Interestingly, in comparison to the LJ model, the Exp-6 model describes the experimental data much better in adsorption on graphite surface for all temperatures examined. In the Henry constant region, the fluid-solid potential plays a significant role in the difference. Therefore, the Exp-6 is better in describing the experimental data because of the, seemingly, more appropriate well depth. As the second layer is formed, this difference is reduced because of the balance between the fluid-solid and fluid-fluid interactions. The LJ model can improve its description of the experimental data by introducing the binary interaction parameter (k_{sf}), while this is not as clearly required for the Exp-6 model.

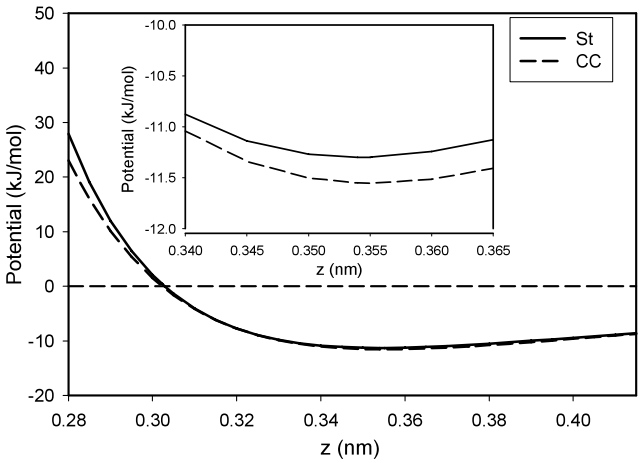

Fig. 3 Potential model of interaction between methane particles and graphite surface. *Inset* shows the well depth of both potential models

Figure 5 shows the isosteric heat of adsorption at 113 K. The Exp-6 model yields a greater isosteric heat in the monolayer coverage region, which is due to the fluid-solid contribution. This result is consistent with what was observed earlier with the isotherms, where the Exp-6 model gives a greater amount adsorbed, resulting higher heat released. From Figures 4 and 5, it can be concluded that the Exp-6 model can describe the experimental adsorption isotherm and isosteric heat better than the LJ model.

We now compare the two models in the description of methane adsorption on graphitic surface under supercritical conditions. Figure 6 illustrate the adsorption isotherms of methane on a graphitized carbon black surface at 298.15 K. It is observed that the Exp-6 model again predicts a higher adsorption at low pressure; less significant at higher pressure. However, at extremely high pressures, the opposite is observed, as shown in the inset of Fig. 6. It shows the effects of the steeper repulsive profile of the Exp-6 model compare to the LJ.

In adsorption in slit pores, the isotherms predicted by both models show a significant difference at low pressures under subcritical and supercritical conditions. Figures 7 and 8 illustrate this behavior at 150 and 200 K. Methane isotherm in 0.65 nm pore was examined to study the difference in the fluid-solid interaction between the two models because in small pores the fluid-solid interaction is dominating. At higher pressures, the opposite behavior was observed. The LJ model predicts significantly greater capacities than the Exp-6 model due to the increasing effects of the repulsive stiffness in the fluid-solid interaction. All the isotherms in 0.65 nm pore show a significant difference at low pressures (Figs. 7a and 8a) which is due to the greater well depth of the Crowell-Chang model (Exp-6 model).

Table 2 The accessible pore volume and width for pore size of 0.65, 0.85, 1.0, and 2.0 nm. The x- and y-box length is 4.0 nm

Pore width (nm)	Pore volume (nm^3)	z_0 (nm)		Accessible pore width (nm)		Percent different[a] (%)
		Exp-6	LJ	Exp-6	LJ	
0.65	10.40	2.8876	2.9063	0.0725	0.0687	5.45
0.85	13.60	2.9762	2.9839	0.2548	0.2532	0.61
1.00	16.00	3.0017	3.0082	0.3997	0.3984	0.33
2.00	32.00	3.0214	3.0276	1.3957	1.3945	0.09

[a]Positive percentage differences show the Exp-6 model is greater

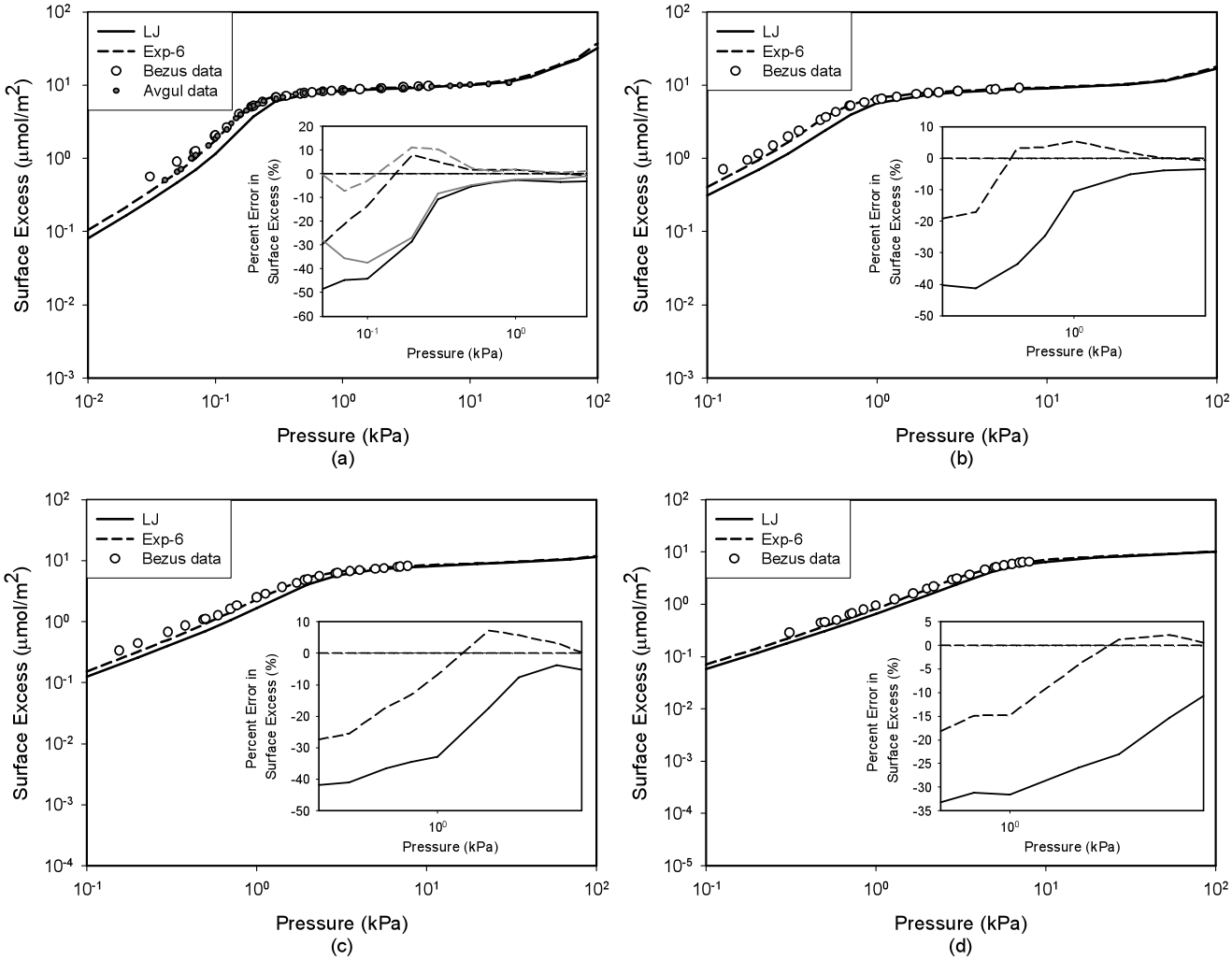

Fig. 4 The fitting of the LJ model and the Exp-6 model with experimental data from Bezus et al. (1967) and Avgul et al. (1970) for methane fluids adsorption at, clockwise from top left, 113, 123, 133 and 143 K on graphitized surface. *Inset* shows the percentage of error

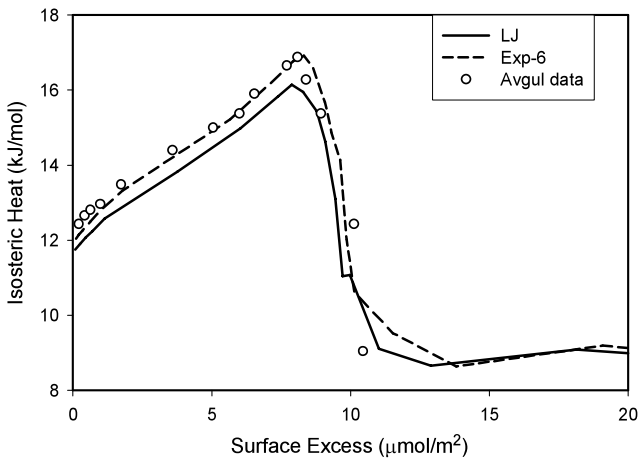

Fig. 5 The isosteric heat of adsorption on graphite surface at 113 K with the experimental data from Avgul (Avgul and Kiselev 1970)

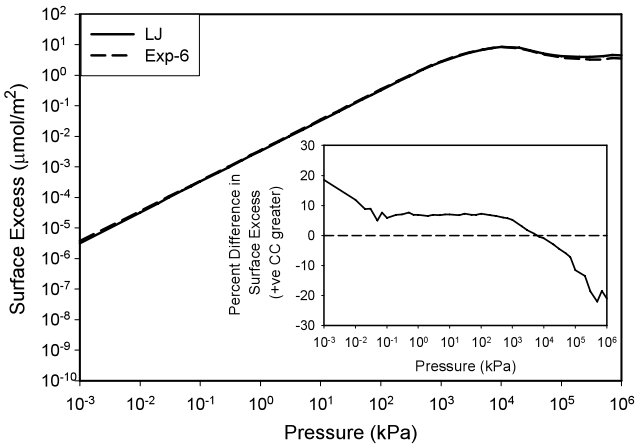

Fig. 6 The isotherm of methane adsorption on graphite surface at 298.15 K. The *inset* shows the percentage difference between the two models

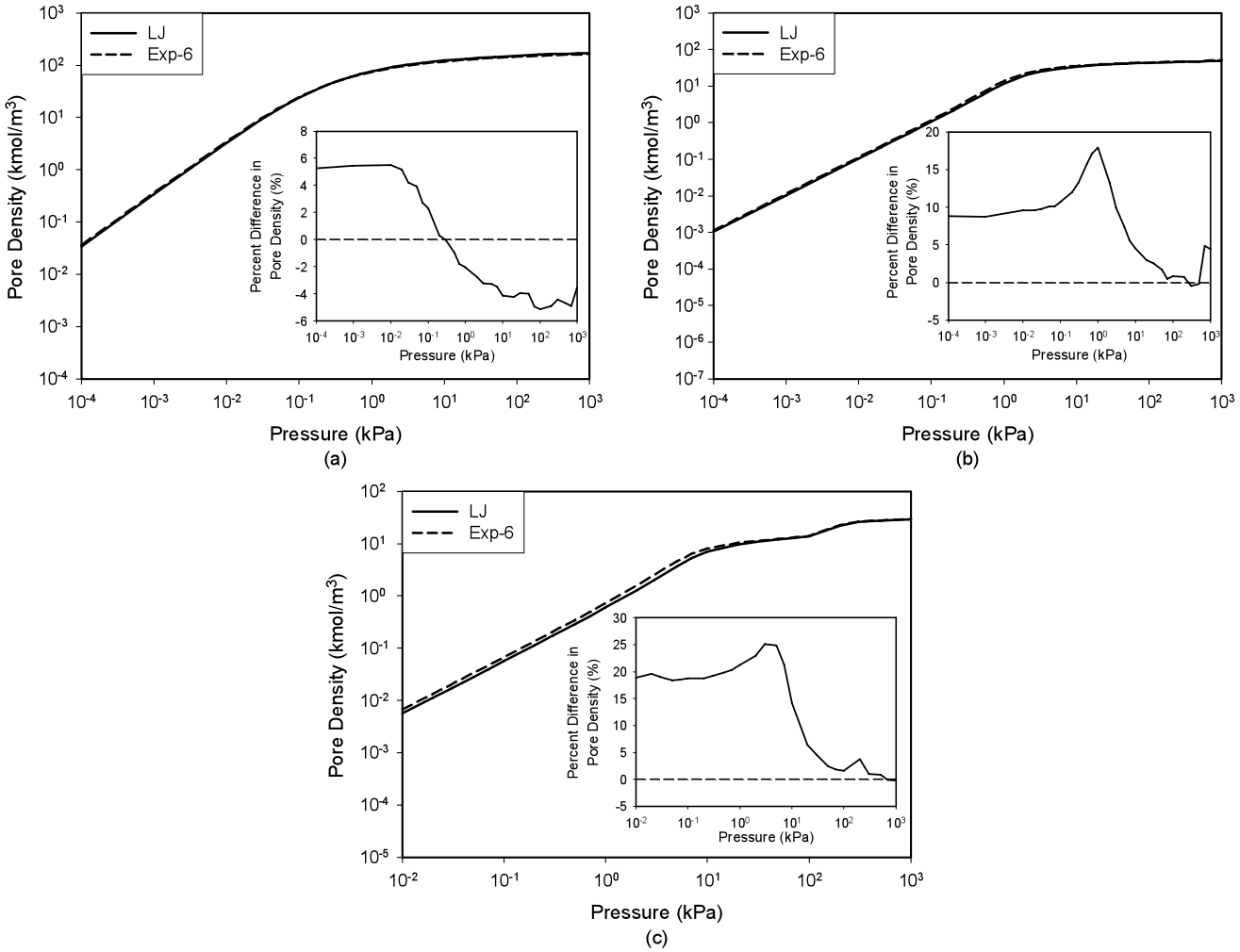

Fig. 7 The isotherm of methane adsorption at 150 K in slit pores of (**a**) 0.65 nm (*single layer*), (**b**) 1.0 nm (*double layers*), and (**c**) 2.0 nm (*multiple layers*). In *inset*, the positive percentage difference means the Exp-6 gives greater capasity

Since the repulsion of the models play a significant role under extremely high pressures, it is generally expected that this is where the two potential models show a difference. The adsorption under supercritical conditions was studied to observe the effects of the difference in the repulsion between the two models at extremely high pressures. The isotherm of methane at 200 K is shown in Fig. 8. The behavior observed is very similar to the behavior under subcritical conditions (150 K), which is shown in Fig. 7. In the adsorption of 0.65 nm pore size, the Exp-6 has predicted, on average, greater capacities at low pressures and the opposite was observed at higher pressures. Whereas, in the adsorption of 1.0 nm and 2.0 nm pores, the Exp-6 has greater capacities than the LJ model at low pressures, and the difference becomes smaller as the pressure increases. Similar behavior was observed in the adsorption isotherm at 298.15 K. These observations suggest that the difference in the repulsion (of the fluid-fluid interaction) does not affect the description of the adsorption isotherm as much in big pores compared with smaller pores.

3.3 Isosteric heat of adsorption

Having seen the difference between the two models on the description of the adsorption isotherms of methane on surface and in pores, the description of isosteric heat is now analyzed. We have presented earlier how well the both models described the isosteric heat of adsorption on graphitic surface under subcritical conditions (see Fig. 5). The isosteric heats of adsorption on a graphitic pore under supercritical are presented in Fig. 9. While the isosteric heat at 113 K obtained for surfaces shows a clear peak that can be attributed to the monolayer completion, this behavior is not seen with the supercritical adsorption at 298.15 K. It can be observed that the Exp-6 model has a greater isosteric heat as under subcritical conditions but the difference between LJ and Exp-6 is smaller.

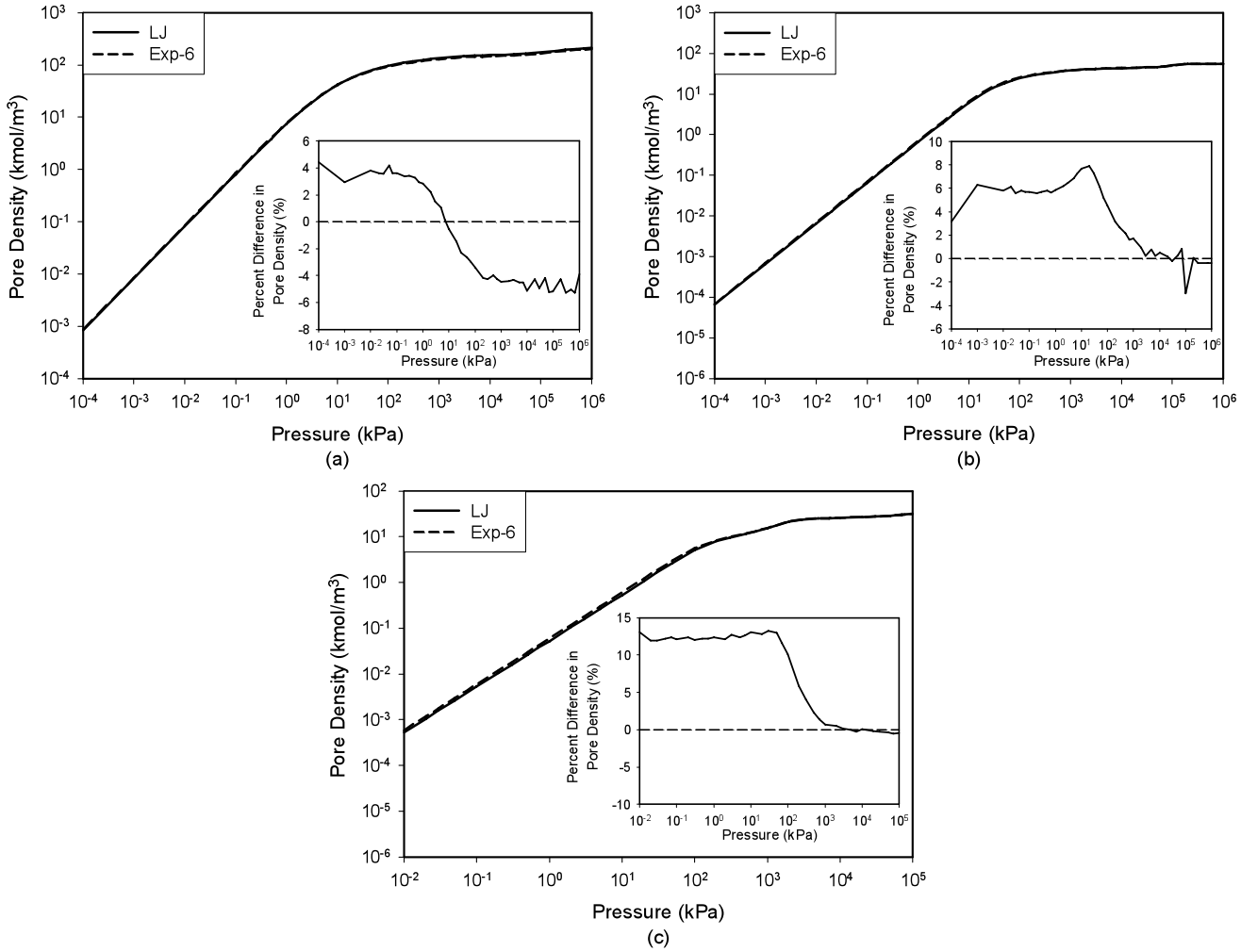

Fig. 8 The isotherm of methane adsorption at 200 K in slit pores of (**a**) 0.65 nm (*single layer*), (**b**) 1.0 nm (*double layers*), and (**c**) 2.0 nm (*multiple layers*). In *inset*, the positive percentage difference means the Exp-6 gives greater capasity

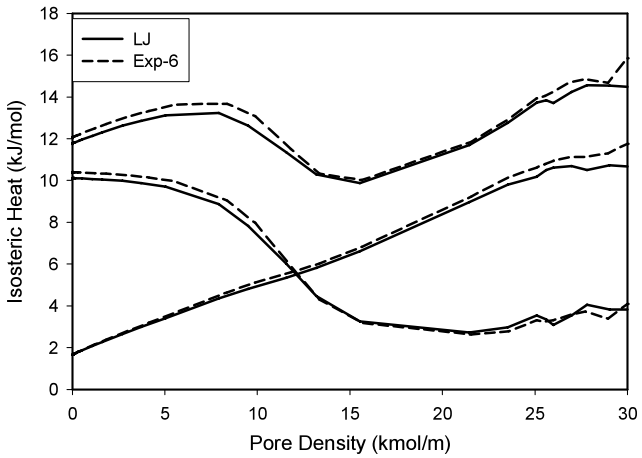

Fig. 9 Isosteric heat of adsorption at 200 K in 2.0 nm pore

4 Conclusion

In this paper, two interaction potential models, Lennard-Jones 12-6 model and the Buckingham Exp-6, are compared in the description of methane in the bulk phase and during adsorption on graphitic surfaces and pores. Both models give a good description of the experimental bulk pressures with higher accuracy for the LJ model at higher densities. In adsorption on graphitic surface, the Exp-6 model fits the experimental adsorption isotherms and isosteric heat of subcritical methane on carbon black better than the LJ model. Further work was done on methane adsorption at different conditions. In the adsorption on surface under supercritical conditions, the Exp-6 predicts higher capacities, however, at extremely high pressures the opposite was observed. For the adsorption in slit pores, two different behaviors were observed from the different pore sizes. In small pore sizes, the Exp-6 model describes a greater capacity at low pressures, while the opposite was observed at high pressures. In larger

pore sizes, both models describe similar capacities at high pressures. Having seen the Exp-6 can describe the experimental data better without any modification, it indicates that the Exp-6 model is a good potential model that researchers can utilized to describe adsorption properties. However, the LJ model is as good as the Exp-6. Therefore, the choice of the potential model can be made based on preference.

Acknowledgement This project is supported by the Australian Research Council.

Appendix A

A.1 The derivation of the Crowell-Chang parameters from the original Exp-6 model

$$\varphi(r) = -Ar^{-6} + B\exp(-\alpha' r)$$

$$\varphi(r) = \frac{\varepsilon}{(1-\frac{6}{\alpha})}\left[\frac{6}{\alpha}\exp\left(\alpha\left(1-\frac{r}{r_m}\right)\right) - \left(\frac{r_m}{r}\right)^6\right]$$

$$\varphi(r) = -\left(\frac{\varepsilon r_m^6}{(1-\frac{6}{\alpha})}\right)r^{-6} + \frac{6\varepsilon}{\alpha(1-\frac{6}{\alpha})}\exp\left(\alpha - \alpha\frac{r}{r_m}\right)$$

$$\varphi(r) = -\left(\frac{\varepsilon r_m^6}{(1-\frac{6}{\alpha})}\right)r^{-6} + \frac{6\varepsilon}{\alpha-6}\exp(\alpha)\exp\left(-\frac{\alpha}{r_m}r\right)$$

The derivation defined Crowell-Chang's parameters as:

$$A = \frac{\varepsilon r_m^6}{(1-\frac{6}{\alpha})}$$

$$B = \frac{6\varepsilon}{\alpha-6}\exp(\alpha)$$

$$\alpha' = \frac{\alpha}{r_m}$$

A.2 The goodness of Pentagamma function approximation

$x(z/\Delta)$	Power series function	Approximation function	Percent difference (%)
1.0	6.49263	6.48828	−0.067
2.0	0.49292	0.48879	−0.837
3.0	0.11813	0.11694	−1.005
4.0	0.04421	0.04398	−0.511
5.0	0.02089	0.02099	0.462
6.0	0.01138	0.01159	1.782
7.0	0.00683	0.00706	3.361
8.0	0.00438	0.00461	5.142
9.0	0.00297	0.00318	7.084
10.0	0.00209	0.00228	9.158

If $z = 2.0$ nm, $\Delta = 0.3354$ nm $\Rightarrow x = 5.9630$ (an approximation of 1.7% percentage difference). Therefore, the approximation function is good

References

Allen, M.P., Tildesley, D.J.: Computer Simulation of Liquids. Oxford University Press, Oxford (1989), pp. xiii, 385

Avgul, N.N., Kiselev, A.V.: Physical adsorption of gases and vapous on graphitized carbon blacks. Chem. Phys. Carbon **6**, 1–124 (1970)

Bezus, A.G., Dreving, V.P., Kiselev, A.V.: Variation with pressure and temperature of adsorption of methane ethane and ethylene on graphitised carbon black. Russ. J. Phys. Chem. **41**(11), 1568–1572 (1967)

Birkett, G., Do, D.D.: New method to determine PSD using supercritical adsorption: applied to methane adsorption in activated carbon. Langmuir **22**, 7622–7630 (2006)

Buckingham, R.A.: The classical equation of state of gaseous helium, neon and argon. Proc. R. Soc. Lond. Ser. A, Math. Phys. Sci. **168**(933), 264–283 (1938)

Crowell, A.D., Chang, C.O.: Constants for a (Exp-6) potential between simple molecules and graphite. J. Chem. Phys. **38**(10), 2584–2586 (1963)

Do, D.D., Do, H.D.: Effects of potential models in the vapor–liquid equilibria and adsorption of simple gases on graphitized thermal carbon black. Fluid Phase Equilib. **236**(1,2), 169–177 (2005)

Duan, Z., Møller, N., Weare, J.H.: Accurate prediction of the thermodynamic properties of fluids in the system H_2O–CO_2–CH_4–N_2 up to 2000 K and 100 kbar from a corresponding states/one fluid equation of state. Geochim. Cosmochim. Acta **64**(6), 1069–1075 (2000)

Errington, J.R., Panagiotopoulos, A.: Phase equilibria of the modified Buckingham Exponential-6 potential from Hamiltonian scaling grand canonical Monte Carlo. J. Chem. Phys. **109**(3), 1093–1100 (1998)

Frenkel, D., Smit, B.: Understanding Molecular Simulation: From Algorithms to Applications. Academic Press, San Diego (1996), pp. xviii, 443

Galliero, G., Boned, C.: Molecular dynamics study of the repulsive form influence of the interaction potential on structural, thermodynamic, interfacial, and transport properties. J. Chem. Phys. **129**(7), 074506-9 (2008)

Kaplan, I.G., Piela, L.: Intermolecular interactions: physical picture, computational methods and model potentials. Phys. Today **60**(7), 64 (2007)

Kowalczyk, P., et al.: Grand canonical Monte Carlo simulation study of methane adsorption at an open graphite surface and in slitlike carbon pores at 273 K. Langmuir **21**(12), 5639–5646 (2005)

Linstrom, P.J., Mallard, W.G.: NIST Chemistry WebBook (2001). Available from: http://webbook.nist.gov

Martin, M.G., Siepmann, J.I.: Transferable potentials for phase equilibria. 1. united-atom description of *n*-alkanes. J. Phys. Chem. B **102**(14), 2569–2577 (1998)

Nicholson, D., Parsonage, G.: Computer Simulation and the Statistical Mechanics of Adsorption. Academic Press, London (1982)

Paricaud, P., et al.: From dimer to condensed phases at extreme conditions: accurate predictions of the properties of water by a Gaussian charge polarizable model. J. Chem. Phys. **122**(24), 244511–244514 (2005)

Ree, F.H.: Simple mixing rule for mixtures with Rxp-6 interactions. J. Chem. Phys. **78**(1), 409–415 (1983)

Ross, M., Ree, F.H.: Repulsive forces of simple molecules and mixtures at high density and temperature. J. Chem. Phys. **73**(12), 6146–6152 (1980)

Setzmann, U., Wagner, W.: A new equation of state and tables of thermodynamic properties for methane covering the range from the melting line to 625 K at pressure up to 1000 MPa. J. Phys. Chem. **20**(6), 1061–1155 (1991)

Sherwood, A.E., Prausnitz, J.M.: Intermolecular potential functions and the second and third virial coefficients. J. Chem. Phys. **41**(2), 429–437 (1964)

Steele, W.A.: The physical interaction of gases with crystalline solids. I. Gas-solid energies and properties of isolated adsorbed atoms. Surf. Sci. **36**(1), 317–352 (1973)

Tavares, F.W., Sandler, S.I.: Vapour-liquid equilibria of exponential-six fluids. Mol. Phys. **87**(6), 1471–1476 (1996)

Vortler, H.L., Nezbeda, I., Lisal, M.: The Exp-6 potential fluid at very high pressures: computer simulations and theory. Mol. Phys. **92**(5), 813–824 (1997)

Wu, G.-W., Sadus, R.J.: Molecular simulation of the high-pressure phase equilibria of binary atomic fluid mixtures using the Exponential-6 intermolecular potential. Fluid Phase Equilib. **170**(2), 269–284 (2000)

Zarragoicoechea, G.J., Scalise, O.H.: On the gas-gas equilibria of second kind of nonpolar fluid binary mixtures from a hard-sphere Exp-6 molecular model. J. Chem. Phys. **107**(11), 4358–4363 (1997)